

# Adding low-cost passive toe joints to the feet structure of SURENA III humanoid robot

Majid Sadedel<sup>†</sup>, Aghil Yousefi-Koma<sup>†, \*</sup>,  
Majid Khadiv<sup>‡</sup> and Mohhamad Mahdavian<sup>†</sup>

<sup>†</sup>*Center of Advanced Systems and Technologies (CAST), School of Mechanical Engineering, College of Engineering, University of Tehran, Tehran, Iran. E-mails: majid.sadedel@ut.ac.ir, m.mahdavian@ut.ac.ir*

<sup>‡</sup>*Center of Excellence in Robotics and Control, Advanced Robotics & Automated Systems (ARAS) Lab, Department of Mechanical Engineering, K. N. Toosi University of Technology, Tehran, Iran. E-mail: mkhadiv@mail.kntu.ac.ir*

(Accepted July 21, 2016. First published online: November 22, 2016)

## SUMMARY

Adding active toe joints to a humanoid robot structure has lots of difficulties such as mounting a small motor and an encoder on the robot feet. Conversely, adding passive toe joints is simple, since it only consists of a spring and a damper. Due to lots of benefits of implementing passive toe joints, mentioned in the literature, the goal of this study is to add passive toe joints to the SURENA III humanoid robot which was designed and fabricated at the Center of Advanced Systems and Technologies (CAST), University of Tehran. To this end, a simple passive toe joint is designed and fabricated, at first. Then, stiffness and damping coefficients are calculated using a vision-based measurement. Afterwards, a gait planning routine for humanoid robots equipped with passive toe joints is implemented. The tip-over stability of the gait is studied, considering the vibration of the passive toe joints in swing phases. The multi-body dynamics of the robot equipped with passive toe joints are presented using the Lagrange approach. Furthermore, system identification routine is adopted to model the dynamic behaviors of the power transmission system. By adding the calculated actuating torques for these two models, the whole dynamic model of the robot is computed. Finally, the performance of the proposed approach is evaluated by several simulations and experimental results. Results show that using passive toe joints reduces energy consumption of ankle and knee joints by 15.3% and 9.0%, respectively. Moreover, with relatively large values of stiffness coefficients, the required torque and power of the knee and hip joints during heel-off motion reduces as the ankle joint torque and power increases.

**KEYWORDS:** Humanoid robot, Passive toe joints, Dynamic model, System identification, Parametric analysis.

## 1. Introduction

SURENA III is the third generation of the humanoid robot which has been designed and fabricated at CAST. SURENA III is capable of walking on straight and curved paths, walking up and down stairs and inclined terrains, and it also uses an online adaptation method on the surfaces with height uncertainties. Besides, the robot can detect objects and faces, recognize voices (in Persian), imitate human motions and perform autonomous actions based on audio and video signals.

A conventional humanoid robot like SURENA III has six rotational degrees of freedom (DoF) in each leg including three-DoF in hip (in  $x$ ,  $y$ , and  $z$  directions), one-DoF in knee (in  $y$  direction) and two-DoF in ankle (in  $x$  and  $y$  directions) according to Fig. 1. However, some humanoid robots

\* Corresponding author. E-mail: aykoma@ut.ac.ir

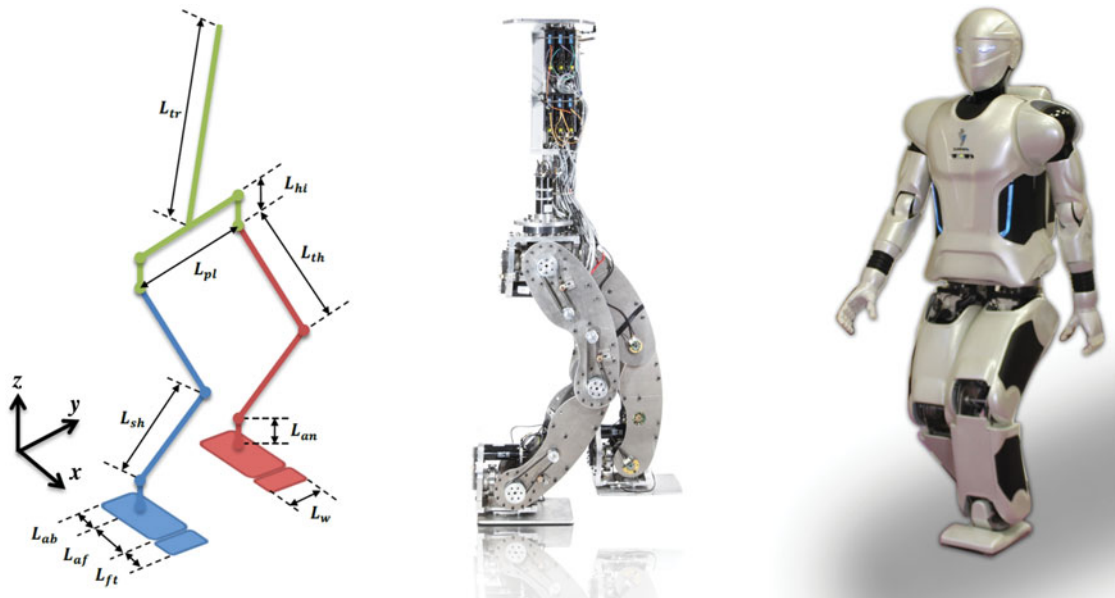


Fig. 1. Humanoid robot SURENA III.

have one additional DoF in their toes. H7,<sup>1</sup> Lola,<sup>2</sup> Toyota<sup>3</sup> and HRP-4C<sup>4</sup> have active toe joints while Wabian-2R,<sup>5</sup> Petman<sup>6</sup> and HRP-2LT<sup>7</sup> have passive toe joints.

Using active toe joints has some advantages such as reaching higher speeds during walking,<sup>1</sup> step height augmentation,<sup>8</sup> stability enhancement,<sup>9,10</sup> energy saving,<sup>11</sup> maximum joint velocity reduction<sup>9</sup> and resemblance to human gait.<sup>4</sup> In this regard, Handharu *et al.* developed a walking pattern with stretched knee motion using active toe and heel joints.<sup>12</sup> Kouchaki *et al.* investigated the standing balance control of a biped robot with active toe joints.<sup>13</sup> Effects of passive toe joints in humanoid field have been addressed as well and faster and smoother walking has been reported as advantages.<sup>5,14</sup> Also, Zhu *et al.* and Sun *et al.* indicated that adding proper passive toe joints could benefit the energy efficiency of ankle joint as well as the stability of the gait.<sup>15,16</sup> Kajita *et al.* developed a running pattern for HRP-2LT equipped with toe springs.<sup>7</sup> Moreover, Kumar *et al.* introduced a hybrid toe joint which is an active joint with a spring and a damper mechanism, to reduce the maximum required torque for this joint.<sup>17</sup>

Mounting a motor and an encoder on a toe joint makes the foot to be heavier, which then leads to leg vibration during motion. Beside from design and fabrication difficulties, it changes the electronic architecture as well. Hence, it is not practical to add active toe joints to an available humanoid robot structure. However, by adding a simple rotary spring and a damper to the robot foot structure, an effective passive toe joint is attainable. According to the benefits of implementing passive toe joints, mentioned in the literature, the aim of this study is to equip SURENA III humanoid robot with passive toe joints, and to investigate the effects of this modification. To this end, a passive toe joint was designed and fabricated. Unlike complicated designs with several links and DoFs,<sup>18–20</sup> a simple joint with proper mechanical characteristic was adopted. In order to calculate the stiffness and damping coefficients, a vision-based measurement routine was exploited.

In the next step, a gait planning routine is presented for humanoid robots equipped with passive toe joints. Adding passive toe joints to the robot structure changes ground reactions. Therefore, the stability of the gait must be checked. There are several stability criteria for humanoid robots including ZMP (Zero Moment Point),<sup>21</sup> FRI (Foot-Rotation Indicator),<sup>22</sup> MFRI (Modified Foot-Rotation Indicator)<sup>23</sup> and CWC (Contact Wrench Condition).<sup>24</sup> In this paper, the ZMP criterion is adopted. To compute the exact location of ZMP, all joint angles are required. Passive toe angle in the under-actuated phases of the gait (swing phases) is unknown. In previous studies, this angle was calculated by solving non-linear differential equations of the dynamic model numerically which is difficult, inaccurate and also time consuming. However, in this paper, this angle is calculated separately using a base-excited vibration model.

Actuator saturation, actuator dead-zone and uncertainty in robot model which leads to unknown dynamics impose some difficulties in experimental tests. He *et al.* studied these challenges and introduced several adaptive neural network methods to deal with these problems.<sup>25–27</sup> Neural dynamic method is also used for dual-arm motion generation to remedy the joint angle drift phenomenon of a humanoid robot.<sup>28</sup>

It is essential to develop an accurate dynamic model in order to analyze humanoid gaits. Furthermore, hardware selection<sup>2,29</sup> and optimization procedures need an accurate dynamic model. There are several goal functions for the optimization procedure, including energy consumption,<sup>30,31</sup> actuating joint torque,<sup>32,33</sup> time of motion<sup>34</sup> and required friction coefficient.<sup>35,36</sup> All these goal functions are calculated based on a dynamic model. Lagrange<sup>37–39</sup>, Newton–Euler<sup>40–42</sup> and Kane<sup>43</sup> are well-known methods for modeling of multi-body dynamics of humanoid robots. Power transmission system was considered ideal in most of those studies. However, in this paper, to obtain an accurate dynamic model, a combination of the Lagrange method and the system identification approach is adopted. The Lagrange method is used for modeling of non-linear and phase dependent multi-body dynamics of the robot equipped with the passive toe joints. The system identification approach is utilized to simplify the complexity of the power transmission system components modeling. Finally, total required joint torque, which is a summation of the output of these two models is obtained.

Several simulations and experimental tests on SURENA III are carried out to verify the presented dynamic model. Also, a comparison between a gait of a robot with and without toe joint is presented to emphasize the benefits of implementing passive toe joints. Finally, several parametric analyses are carried out to investigate the effects of large values of stiffness and damping coefficients on joint torques and powers during heel-off motion.

## 2. Passive Toe Joint: Design and Identification

In this section, the design and parameter identification of the passive toe joint including stiffness and damping coefficients are presented. The goal is to design a simple, light and effective passive toe joint which is easy to fabricate without necessity of an encoder. The presented passive toe joint is illustrated in Fig. 2. For simplicity, a thin metal plane is used to add elasticity to the toe joint. However, the combination of a rotary spring and a damper can be used as an alternative.

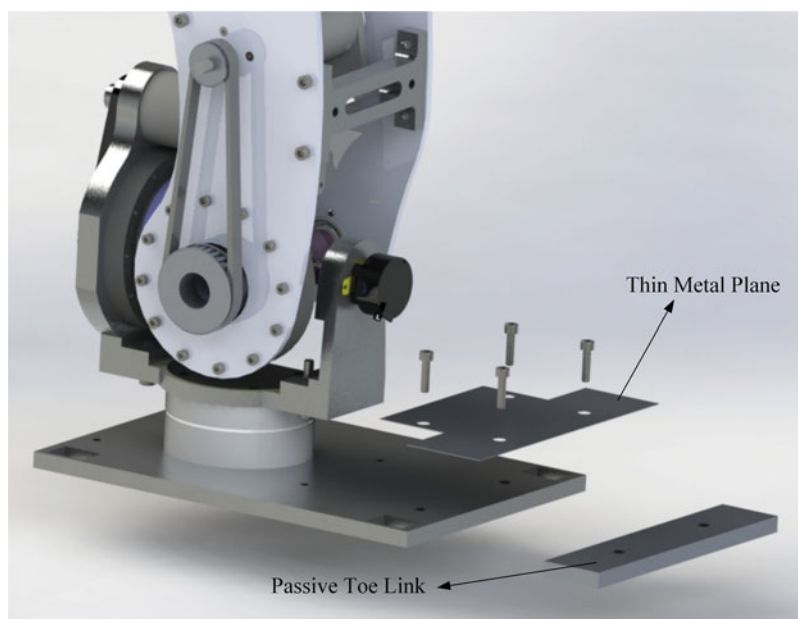


Fig. 2. Exploded view of the proposed passive toe joint.

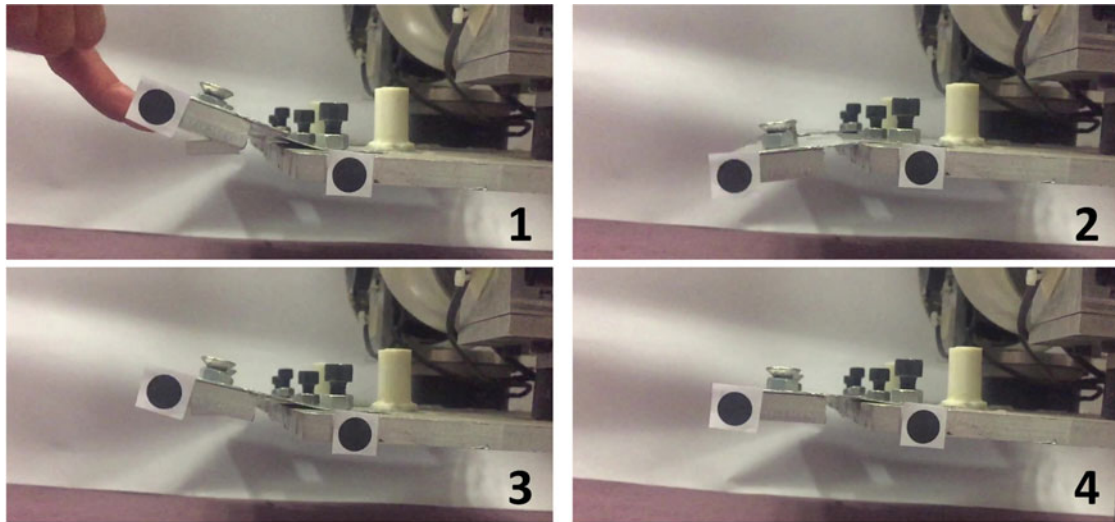


Fig. 3. The toe angle is calculated based on the positions of two markers.

A free vibration test with the position as the initial condition is adopted for the system identification procedure. Since there is no encoder in the joint, a vision-based measurement is exploited to determine the toe angle. According to Fig. 3, the positions of two marker centers are calculated in pixels for each frame of the test video using “Vision Express” module in LabVIEW. Since the camera and the foot are fixed, given the marker positions, the toe angle can be calculated by  $\tan^{-1}(\frac{\Delta y}{\Delta x})$ .

The toe angle extracted from vision-based measurement is illustrated in Fig. 4. It can be seen that the passive toe joint has an under-damped response. Therefore, the natural frequency ( $\omega_n$ ) and

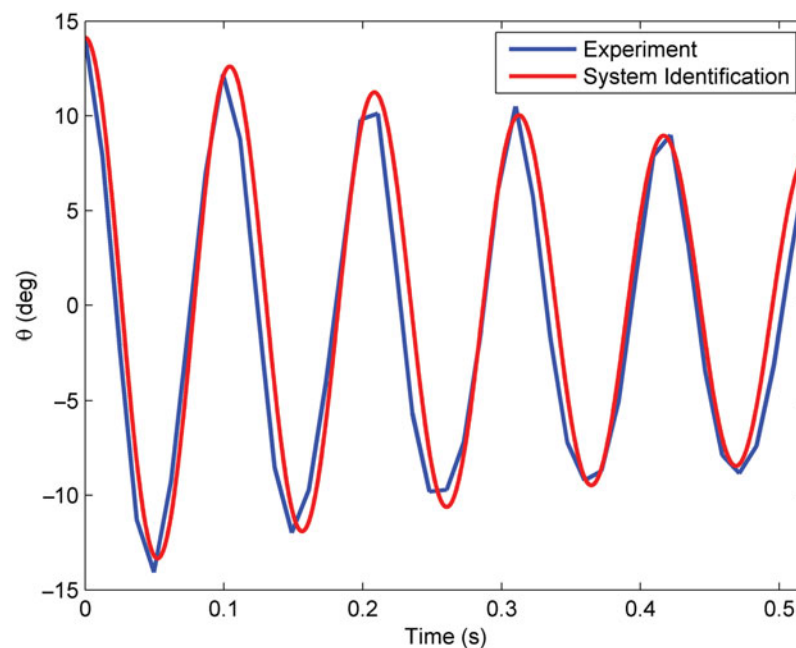


Fig. 4. The toe angle calculated using vision-based experiment and system identification approach.

damping ratio ( $\zeta$ ) can be determined using “Logarithmic Decrement formula”:<sup>44</sup>

$$\begin{aligned}
 T &= \frac{(t_n - t_0)}{n}, \\
 \delta &= \frac{1}{n} \log \left( \frac{\theta(t_0)}{\theta(t_n)} \right), \\
 \omega_n &= \sqrt{\frac{K}{J}} = \frac{\sqrt{4\pi^2 + \delta^2}}{T}, \\
 \zeta &= \frac{C}{2\sqrt{KJ}} = \frac{\delta}{\sqrt{4\pi^2 + \delta^2}},
 \end{aligned}
 \tag{1}$$

where  $t_n$  is the time at which the  $n$  th peak occurs. Considering the five cycles which are illustrated in Fig. 4,  $\omega_n$  and  $\zeta$  are obtained as  $60.3324(\frac{\text{rad}}{\text{sec}})$  and  $0.0181$ , respectively ( $R^2 = 0.9704$ ). Given the toe link moment of inertia, stiffness ( $K$ ) and damping ( $C$ ) coefficients are  $0.6938(\frac{\text{N.m}}{\text{rad}})$  and  $0.0004(\frac{\text{N.m.sec}}{\text{rad}})$ , respectively.

### 3. Gait Generation

This gait generation routine is based on the position ( $x$ ,  $y$  and  $z$ ) of the ankle and hip joints and the orientation (roll, pitch and yaw) of the foot and pelvis links in the task space. The description of the gait parameters is presented in Table I. Also, visual representations of path planning parameters in the sagittal and coronal planes are depicted in Figs. 5 and 6, respectively.

According to Fig. 5, roll and yaw orientations of the feet are assumed to be zero. Pitch orientation of right foot has the following constraints:

$$\beta_{fr} = \begin{cases} 0 & 0 \leq t \leq T_{dm2} \\ Q_{fb} & t = T_d \\ Q_{fm} & t = T_d + T_{sm} \\ Q_{ff} & t = T_c \\ 0 & T_c + T_{dm1} \leq t \leq 2T_c \end{cases} .
 \tag{2}$$

Table I. Description of the gait parameters.

Parameters	Description
$D_c$	Stride length
$T_c$	Walking cycle time
$T_d$	Double support (DS) time
$T_s$	Single support (SS) time
$T_{sm}$	Middle time in SS in which the position of ankle in $z$ direction is maximum
$T_{dm1}$	First middle time in DS in which the foot rotation around heel ends
$T_{dm2}$	Second middle time in DS in which the foot rotation around toe starts
$Z_{am}$	Position of ankle in $z$ direction at $T_{sm}$
$Q_{fm}$	Angle of swing foot with respect to the ground at $T_{sm}$
$Q_{fb}$	Angle of toe rotation at the end of DS
$Q_{ff}$	Angle of heel rotation at the start of DS
$X_{ed}$	Distance of the pelvis and stance ankle in $x$ direction at the end of SS
$X_{sd}$	Distance of the pelvis and stance ankle in $x$ direction at the start of SS
$Y_{pl_{max}}$	Position of pelvis in $y$ direction at the middle of SS which is maximum
$Y_{pl_d}$	Position of pelvis in $y$ direction at the start of DS
$Z_{pl_{max}}$	Position of pelvis in $z$ direction at the middle of SS which is maximum
$Z_{pl_{min}}$	Position of pelvis in $z$ direction at the middle of DS which is minimum

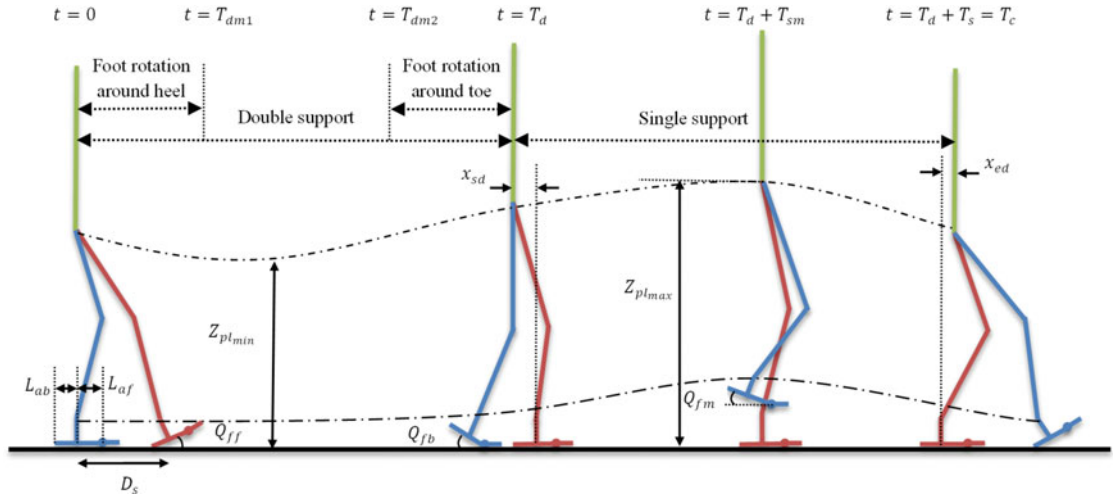


Fig. 5. Visual representation of path planning parameters in the sagittal plane.

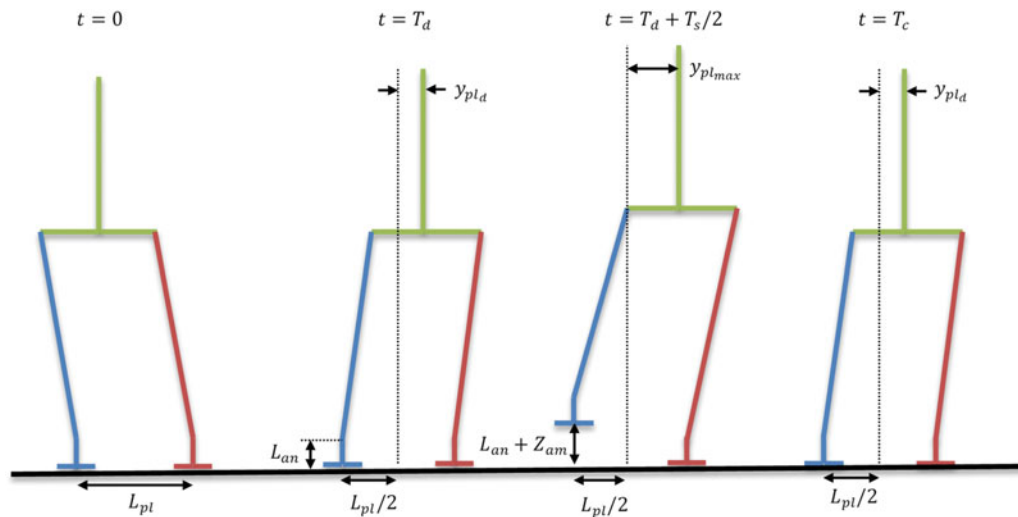


Fig. 6. Visual representation of the path planning parameters in the coronal plane.

Moreover, the position of right ankle in  $x$  and  $z$  directions has these constraints:

$$x_{ar} = \begin{cases} 0 & 0 \leq t \leq T_{dm2} \\ L_{af} (1 - \cos(Q_{fb})) + L_{an} \sin(Q_{fb}) & t = T_d \\ 2D_c - L_{ab} (1 - \cos(Q_{ff})) + L_{an} \sin(Q_{ff}) & t = T_c \\ 2D_c & T_c + T_{dm1} \leq t \leq 2T_c \end{cases}, \quad (3)$$

$$z_{ar} = \begin{cases} L_{an} & 0 \leq t \leq T_{dm2} \\ L_{af} \sin(Q_{fb}) + L_{an} \cos(Q_{fb}) & t = T_d \\ L_{an} + Z_{am} & t = T_d + T_{sm} \\ -L_{ab} \sin(Q_{ff}) + L_{an} \cos(Q_{ff}) & t = T_c \\ L_{an} & T_c + T_{dm1} \leq t \leq 2T_c \end{cases}. \quad (4)$$

It should be noted that the distance between the ankle joints in the lateral direction is considered to be constant ( $L_{pl}$ ) in order to avoid self-collision of the legs (Fig. 6).

Also, to gain simplicity, roll, pitch and yaw orientations of the pelvis are assumed to be zero. The position of right hip in  $x$ ,  $y$  and  $z$  directions has these constraints:

$$x_p = \begin{cases} x_{ed} & t = 0 \\ D_c - x_{sd} & t = T_d \\ D_c + x_{ed} & t = T_c \\ 2D_c - x_{sd} & t = T_c + T_d \\ 2D_c + x_{ed} & t = 2T_c \end{cases}, \tag{5}$$

$$y_p = \begin{cases} -Y_{pl_d} & t = 0 \\ Y_{pl_d} & t = T_d \\ Y_{pl_{max}} & t = T_d + T_s/2 \\ Y_{pl_d} & t = T_c \\ -Y_{pl_d} & t = T_c + T_d \\ -Y_{pl_{max}} & t = T_c + T_d + T_s/2 \\ -Y_{pl_d} & t = 2T_c \end{cases}, \tag{6}$$

$$z_p = \begin{cases} Z_{pl_{min}} & t = T_d/2 \\ Z_{pl_{max}} & t = T_d + T_s/2 \\ Z_{pl_{min}} & t = T_c + T_d/2 \\ Z_{pl_{max}} & t = T_c + T_d + T_s/2 \end{cases}. \tag{7}$$

Smooth spline trajectories with velocity and acceleration continuity are generated to satisfy these constraints. Given these trajectories in task space, the trajectories in joint space are calculated using inverse kinematics (IK).<sup>45</sup> It should be noted that the angle of the passive toe joint is still unknown and will be calculated in Section 4.

#### 4. Stability of the Gait

Adding passive toe joints changes the dynamic behavior of the humanoid robot. In other words, the ground reactions, joint torques and energy consumption will be different. The question is “*Is the gait still stable after adding the passive toe joints?*” To answer this question, the ZMP criterion is adopted to determine the tip-over stability. The position of the ZMP can be calculated as follows:<sup>46</sup>

$$\begin{aligned} X_{ZMP} &= \frac{\sum_{i=1}^n x_{G_i} \times m_i (\ddot{z}_{G_i} + g) - \sum_{i=1}^n z_{G_i} \times m_i \ddot{x}_{G_i} - \sum_{i=1}^n \bar{I}_{y_i} \ddot{q}_{y_i}}{\sum_{i=1}^n m_i (\ddot{z}_{G_i} + g)}, \\ Y_{ZMP} &= \frac{\sum_{i=1}^n y_{G_i} \times m_i (\ddot{z}_{G_i} + g) - \sum_{i=1}^n z_{G_i} \times m_i \ddot{y}_{G_i} - \sum_{i=1}^n \bar{I}_{x_i} \ddot{q}_{x_i}}{\sum_{i=1}^n m_i (\ddot{z}_{G_i} + g)}, \end{aligned} \tag{8}$$

where  $n$  is the number of robot links. According to Eq. (8), all joint angles including toe angles must be known in order to calculate the ZMP position. The toe angle in the stance phase is equal to the angle of sole with respect to the ground which can be computed using forward kinematics. Conversely, in the swing phase, the toe angle is unknown since the joint is passive and can freely vibrate. The only way to use the ZMP criterion for this under-actuated phase of the gait is to calculate the passive toe angle. In other studies, this angle is determined by solving the non-linear differential equations of dynamic model numerically. Apart from the difficulties of this method, the ground reaction forces in a dynamic model depend on the ZMP location itself. In this paper, on the other hand, the angle of the passive toe joint is calculated separately and independently from the whole body dynamics. The trick to do so is to consider the motion of the toe link in the swing phase as a base-excited vibration. The sole link is given a prescribed motion which can be calculated using forward kinematics, causing the toe link to vibrate. A 2D model of this vibration is illustrated in Fig. 7.

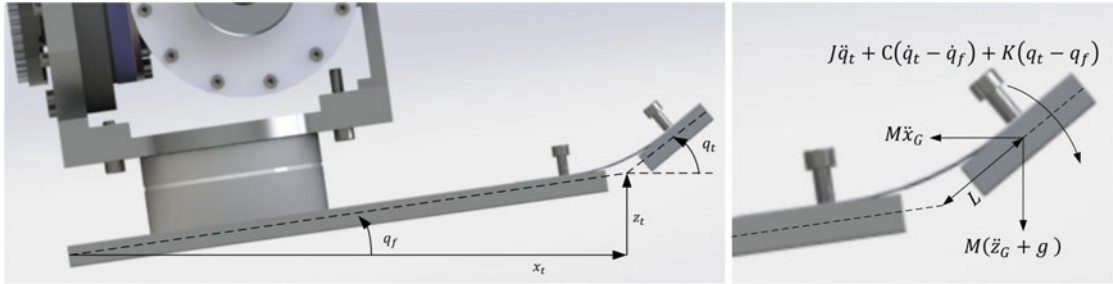


Fig. 7. The motion of the toe link in swing phase is considered as a base-excited vibration.

The governing equation of motion of the toe link in the swing phase can be stated in the following form:

$$\begin{cases} \ddot{x}_G = \ddot{x}_t - L\ddot{q}_t \sin(q_t) - L\dot{q}_t^2 \cos(q_t) \\ \ddot{z}_G = \ddot{z}_t + L\ddot{q}_t \cos(q_t) - L\dot{q}_t^2 \sin(q_t) \\ J\ddot{q}_t + C(\dot{q}_t - \dot{q}_f) + K(q_t - q_f) + M(\ddot{z}_G + g)L \cos(q_t) - M\ddot{x}_G L \sin(q_t) = 0 \end{cases} \quad (9)$$

$$\Rightarrow (J + ML^2)\ddot{q}_t + C\dot{q}_t + Kq_t + M(\ddot{z}_t + g)L \cos(q_t) - M\ddot{x}_t L \sin(q_t) = C\dot{q}_f + Kq_f$$

Given  $\ddot{x}_t$ ,  $\ddot{z}_t$ ,  $q_f$  and  $\dot{q}_f$  using forward kinematics, the toe joint angle in the swing phase can be determined. Now, speaking about stability itself, ZMP can be calculated by substituting the toe joint angle in the Eq. (8).

### 5. Dynamic Modeling

In this section, dynamic modeling of the humanoid robot with passive toe joints is investigated. The presented dynamic model consists of two parts. In the first part, multi-body dynamics of the robot is calculated. For more accurate models, power transmission system is modeled using a system identification approach which is presented in the second part.

#### 5.1. Multi-body dynamics

In this section, a multi-body dynamic model for different walking phases is presented. According to the ZMP criterion, the robot must be fully actuated in order to be stable.<sup>21</sup> Therefore, if the ZMP is located under the stance toe in SS (Single Support) phase (Table II Case 1b) or DS (Double Support) phase (Table II Case 3b and 5b), the motion will be unstable. In these cases, the robot can freely rotate around the passive toe joint. These cases are illustrated in Table II tagged as “Unstable”. The SS phase on the toe link (Table II Case 2) is similar to foot rotation around its tip for the robots without the toe joint. In this case, the support polygon is just a line and therefore, the motion is stable only if the ZMP is located on this line which is practically not feasible.

Using the Lagrange method, multi-body dynamics equations can be simplified into the following form:<sup>47</sup>

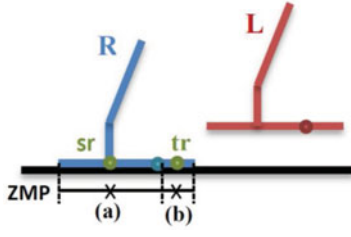
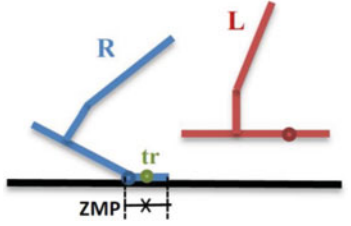
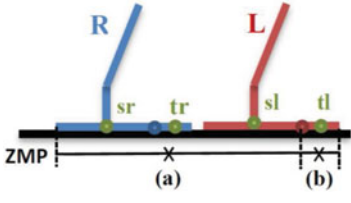
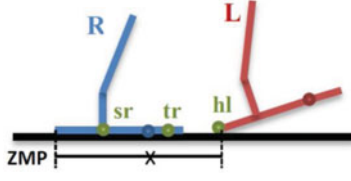
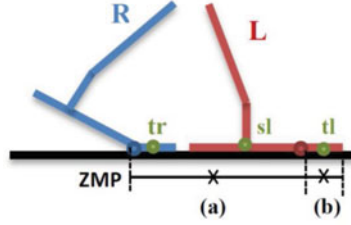
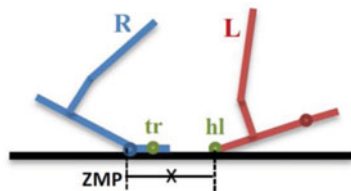
$$M_{20 \times 20}(q)\ddot{q}_{20 \times 1} + V_{20 \times 1}(q, \dot{q}) + G_{20 \times 1}(q) = Q_{20 \times 1}, \quad (10)$$

where  $M(q)$  is the symmetric positive inertia matrix,  $V(q, \dot{q})$  contains the centrifugal and Coriolis terms,  $G(q)$  stands for the gravitational forces and  $q$  and  $Q$  denote the vector of the generalized coordinate and force, respectively. It is noteworthy that  $K$  and  $C$  of the toe spring and damper appear in the left-hand side of Eq. (10).

Active joint torques including hip, knee and ankle can be stated as  $B_{20 \times 12}\tau_{12 \times 1}$  in the generalized force vector. Consistent with the various walking phases, different ground reactions can be calculated using “constraint relaxation method”.<sup>47</sup> Generalized force vector for different walking phases is indicated in Table II. It should be noted that, since the joint torque of the stance passive toe is zero, there exists a ground reaction force toward the  $z$ -direction that compensates the gravity force of the toe link (Table II Case 1a, 3a, 4 and 5a).



Table II. Generalized force vector for different walking phases.

Case	Motion phase	Schema	Ground reactions and generalized force vector
1	SS on right sole		$a) F_{sr} = [F_x, F_y, F_z, M_x, M_y, M_z]^T$ $F_{tr} = [F_z]$ $Q = [B \ J_{sr}^T \ J_{tr}^T]_{20 \times 19} \begin{bmatrix} \tau \\ F_{sr} \\ F_{tr} \end{bmatrix}_{19 \times 1}$ <p>b) Unstable</p>
2	SS on right toe		<p>Unstable</p>
3	DS with both soles		$a) F_{sr} = [F_x, F_y, F_z, M_x, M_y, M_z]^T$ $F_{tr} = [F_z] \ F_{sl} = [F_x, F_y, F_z, M_x, M_y, M_z]^T$ $F_{tl} = [F_z]$ $Q = [B \ J_{sr}^T \ J_{tr}^T \ J_{sl}^T \ J_{tl}^T]_{20 \times 26} \begin{bmatrix} \tau \\ F_{sr} \\ F_{tr} \\ F_{sl} \\ F_{tl} \end{bmatrix}_{26 \times 1}$ <p>b) Unstable</p>
4	DS with right sole and left heel		$F_{sr} = [F_{x_r}, F_{y_r}, F_{z_r}, M_{x_r}, M_{y_r}, M_{z_r}]^T$ $F_{tr} = [F_z]$ $F_{hl} = [F_{x_l}, F_{y_l}, F_{z_l}, M_{x_l}, M_{z_l}]^T$ $Q = [B \ J_{sr}^T \ J_{tr}^T \ J_{hl}^T]_{20 \times 24} \begin{bmatrix} \tau \\ F_{sr} \\ F_{tr} \\ F_{hl} \end{bmatrix}_{24 \times 1}$
5	DS with right toe and left sole		$a) F_{tr} = [F_{x_r}, F_{y_r}, F_{z_r}, M_{x_r}, M_{y_r}, M_{z_r}]^T$ $F_{sl} = [F_{x_l}, F_{y_l}, F_{z_l}, M_{x_l}, M_{y_l}, M_{z_l}]^T$ $F_{tl} = [F_z]$ $Q = [B \ J_{tr}^T \ J_{sl}^T \ J_{tl}^T]_{20 \times 25} \begin{bmatrix} \tau \\ F_{tr} \\ F_{sl} \\ F_{tl} \end{bmatrix}_{25 \times 1}$ <p>b) Unstable</p>
6	DS with right toe and left heel		$F_{tr} = [F_{x_r}, F_{y_r}, F_{z_r}, M_{x_r}, M_{y_r}, M_{z_r}]^T$ $F_{hl} = [F_{x_l}, F_{y_l}, F_{z_l}, M_{x_l}, M_{z_l}]^T$ $Q = [B \ J_{tr}^T \ J_{hl}^T]_{20 \times 23} \begin{bmatrix} \tau \\ F_{tr} \\ F_{hl} \end{bmatrix}_{23 \times 1}$

\*sr: right sole, tr: right toe, hr: right heel, sl: left sole, tl: left toe, hl: left heel.

According to Eq. (10), given the generalized coordinates and its first and second derivatives, a set of linear equations can be obtained. The number of unknown parameters including joint torques and ground reactions is phase dependent. Except for the case 1a, the number of unknowns is greater than the number of equations (i.e. 20). Therefore, the “Moore–Penrose pseudo-inverse method” is adopted to solve Eq. (10):<sup>48</sup>

$$\begin{aligned} Q &= AX \\ M(q)\ddot{q} + V(q, \dot{q}) + G(q) &= AX \Rightarrow X = A^+(M(q)\ddot{q} + V(q, \dot{q}) + G(q)) + (I - A^+A)k \quad (11) \\ k = 0 &\Rightarrow X = A^+(M(q)\ddot{q} + V(q, \dot{q}) + G(q)) \end{aligned}$$

where  $A^+$  represents Moore–Penrose pseudo-inverse of matrix  $A$ ,  $I$  is the identity matrix and  $k$  is an arbitrary constant vector which is chosen to be zero in order to have the minimum norm solution.

According to Table II, for the case 1a (SS phase on sole), the number of unknowns is 19 which is smaller than the number of equations (i.e. 20). In this case, due to the passive toe joint of the swing leg, the system is under-actuated. In other words, the toe angle of the swing leg is unknown. Considering the unknown toe angle, the number of equations and unknowns will be the same (i.e. 20). Therefore, Eq. (10) is a set of non-linear differential equations. In other studies, the multi-body dynamic equations of this case are solved numerically which is difficult, inaccurate and also time consuming. However, in this paper, an explicit solution is adopted. The trick to solve the multi-body dynamic equations for this case is to calculate the toe angle of the swing leg separately using a base-excited vibration model as mentioned in Section 4. Therefore, by substituting the calculated toe angle into the Eq. (10) and eliminating one arbitrary equation, a set of linear algebraic equations will be the result. Since the number of equations and unknowns are the same (i.e. 19), the unknowns can be determined using “Gaussian elimination method”,<sup>49</sup> since this method is more efficient in comparison with “Moore–Penrose pseudo-inverse method” from both execution time and numerical accuracy standpoints.

### 5.2. Power transmission modeling

Since power transmission dynamics is not phase-dependent, an identification approach is exploited in order to simplify the modeling of different components of the so-called power transmission system. The developed power transmission test bench is illustrated in Fig. 8.

After many trials and errors, a model which consists of effective inertia ( $J$ ), viscous friction ( $C$ ) and coulomb friction ( $B$ ) is obtained:

$$\begin{aligned} I &= J\ddot{\theta} + C\dot{\theta} + B\text{sgn}(\dot{\theta}), \\ \tau &= K_i I, \end{aligned} \quad (12)$$

where  $I$  is the motor current,  $\theta$  is the joint angle,  $\text{sgn}$  is the sign function and  $K_i$  is the motor torque constant. The average, standard deviation and consistency measure of model parameters are presented in Table III.<sup>50</sup> Each joint torque is the summation of multi-body dynamics and power transmission model torques.

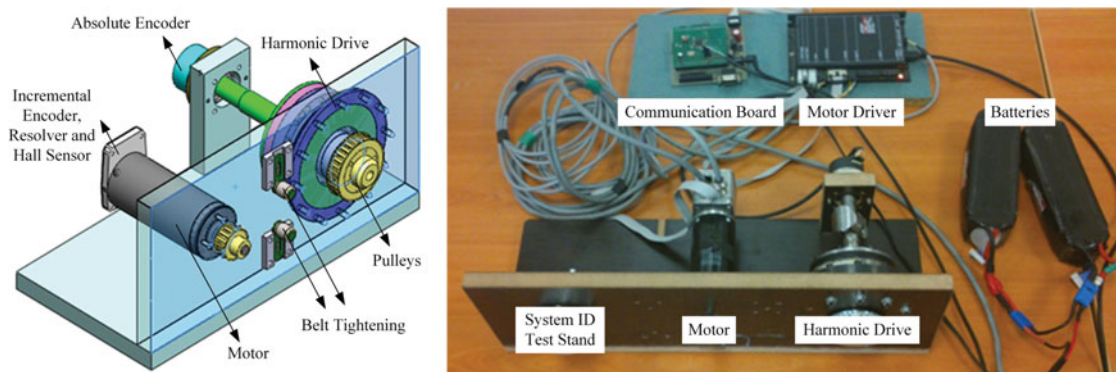


Fig. 8. Power transmission test bench.

Table III. The average, standard deviation and consistency measure of model parameters.

	$J(\text{amp. sec}^2)$	$C(\text{amp. sec})$	$B(\text{amp})$
Average	0.787	5.375	2.852
Standard deviation	0.396	2.153	0.205
Consistency measure	50.34%	40.05%	7.19%

### 6. Results and Discussion

In this section, the simulation and experimental results of the humanoid robot SURENA III are presented. The flowchart of adding passive toe joint procedure is depicted in Fig. 9. After passive

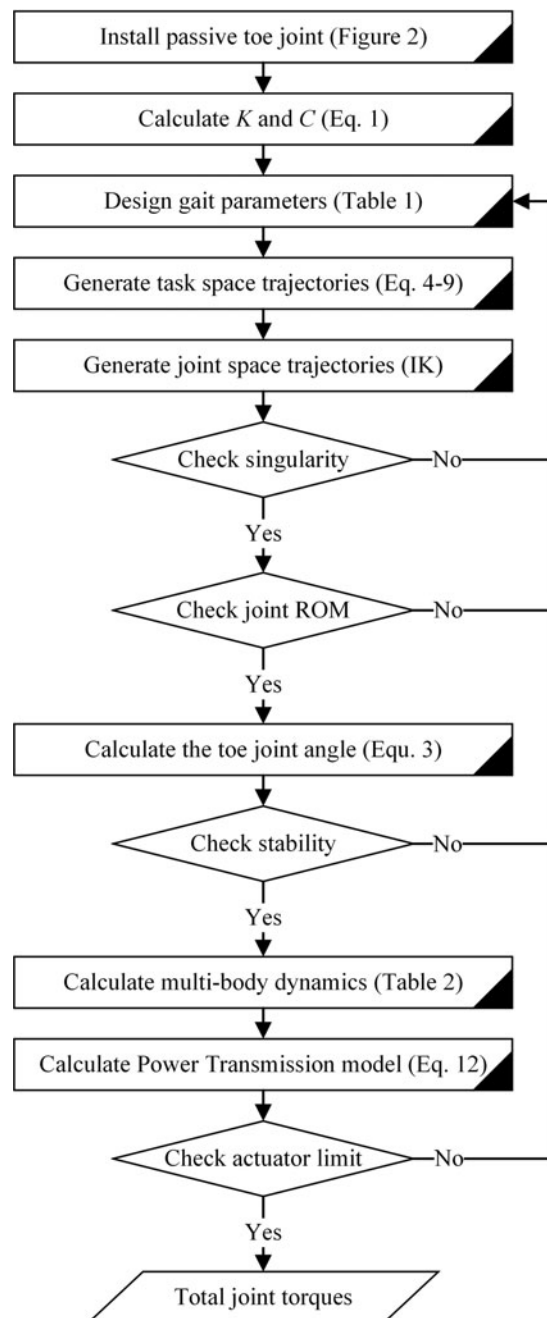


Fig. 9. The flowchart of adding passive toe joint procedure.

toe joints installation, the stiffness and damping coefficients are calculated using a vision-based measurement. Chosen suitable values for gait parameters, path planning trajectories in task space and joint space are determined. After checking knee joint singularity and joint range of motion (RoM), the angles of passive toe joints in DS and SS phases are calculated. Given the passive toe angle, the stability of the gait is verified using the ZMP criterion. Finally, by the adding joint torques calculated using the power transmission model and multi-body dynamics, the total joint torques are determined considering the actuator limits.

### 6.1. Vibration of the passive toe joint in the swing phase

The angle of the passive toe joint in the swing phase for different values of stiffness ( $K$ ) and damping ( $C$ ) coefficients is illustrated in Fig. 10 using Eq. (9). The heel-off motion in which the passive toe joint is bent  $10^\circ$  can be seen at the end of the DS phase. Small values of  $K$  causes low frequency vibrations with high amplitude while large values of  $K$  leads to high frequency and low amplitude vibrations. On the other hand, increasing the value of  $C$  will dissipate the vibration more. Larger values of  $K$  and  $C$  have similar results to the  $K = 10.0$  and  $C = 0.01$ , respectively. The positive rotation of the toe joint at the end of the SS phase is due to weight compensation of the toe link. As  $K$  increases, this rotation angle decreases. Although there is a sudden reduction in the toe angle during transition from SS to DS in simulation results, the toe joint is extended smoothly by reaching toe link to the ground in experimental tests.

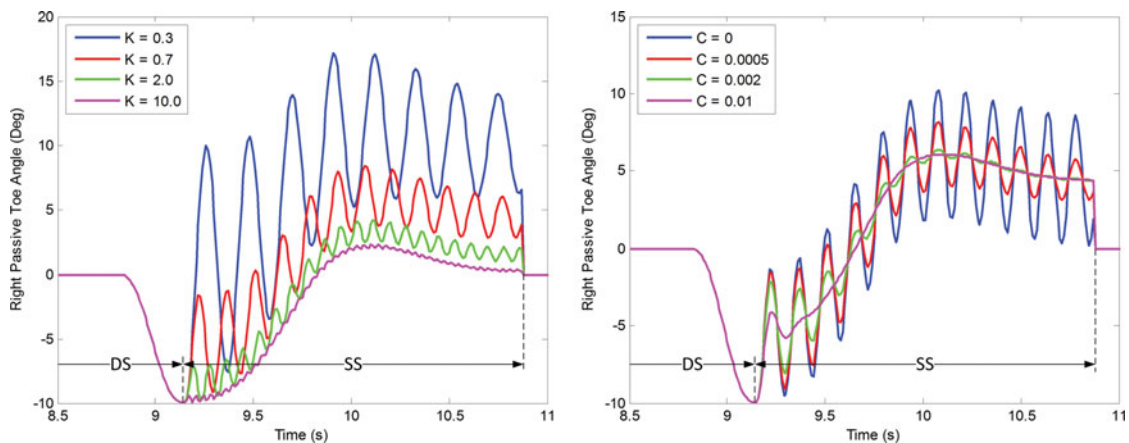


Fig. 10. Effects of different values of  $K$  for  $C = 0.0004$  and different values of  $C$  for  $K = 0.6938$  on the angle of passive toe joint in SS.

### 6.2. Simulation results

The ZMP based on robot kinematics (Eq. (8)) and the ZMP based on ground reactions for a gait with  $10^\circ$  heel-off motion are depicted in Fig. 11. Coincident of ZMPs verifies the multi-body dynamic model calculations. Also, the motion is stable since ZMP trajectory is located inside the support polygon.

### 6.3. Experimental results

To verify the presented dynamics model, a walking test with 40 cm stride length and  $10^\circ$  heel-off motion is implemented on SURENA III. Using a 6-axis force/torque sensor, ZMP trajectory is calculated (Fig. 12). Also, joint torques and powers are obtained by logging motor current feedback

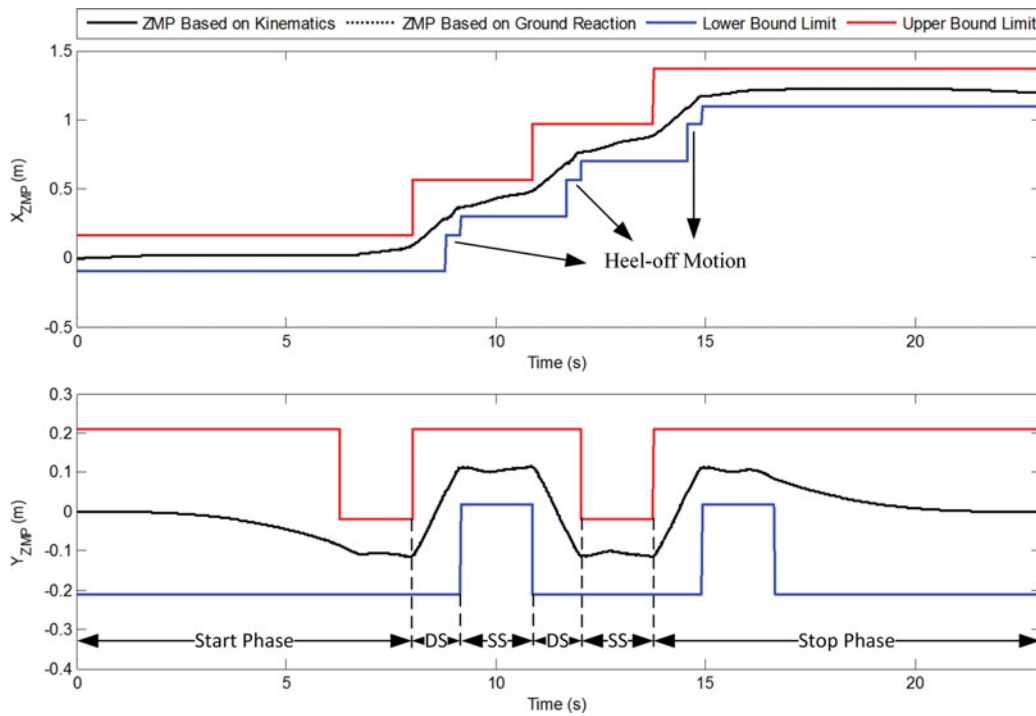


Fig. 11. ZMP based on kinematics and ground reactions.

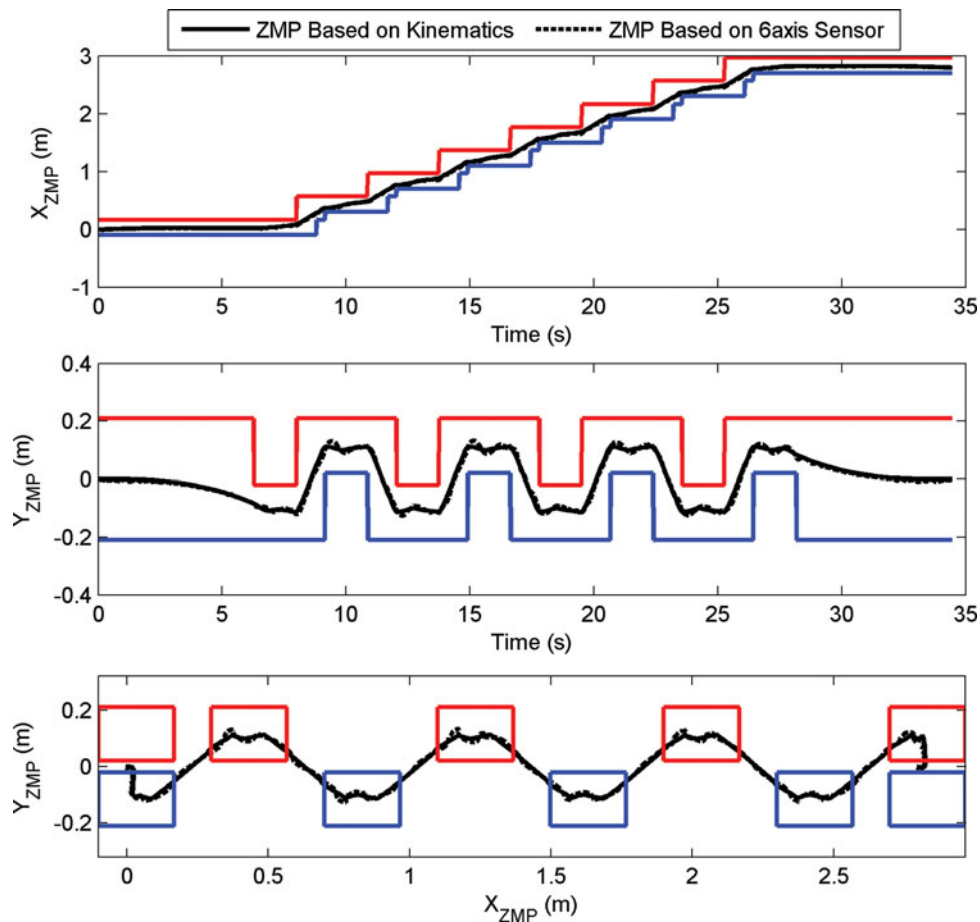


Fig. 12. ZMP based on kinematics and 6-axis sensor.

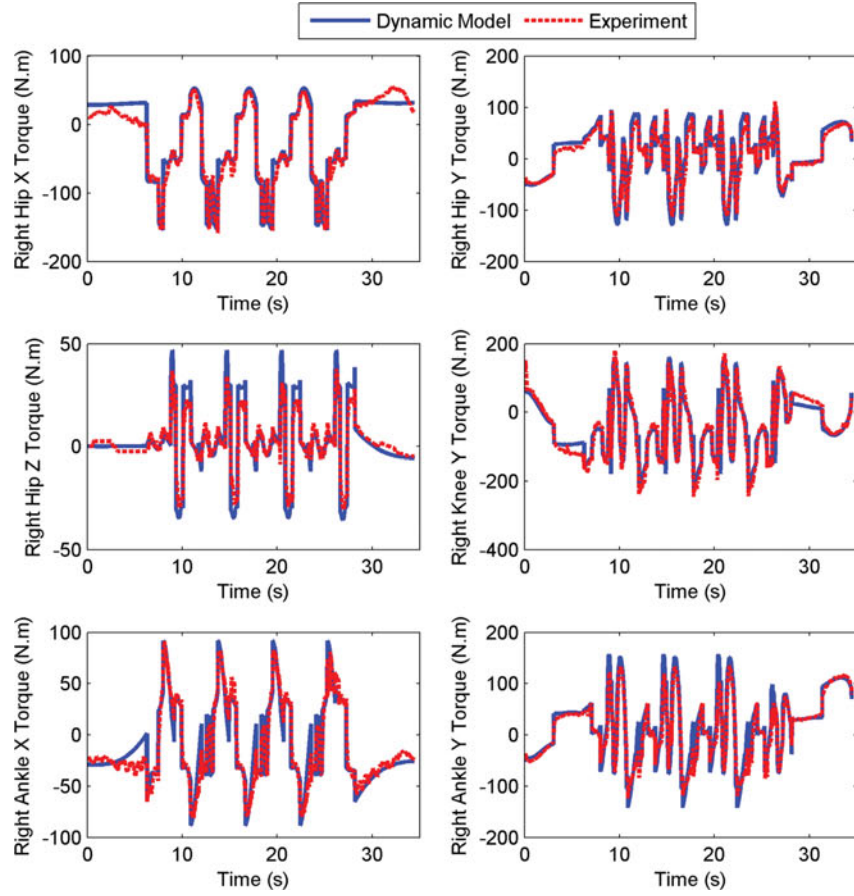
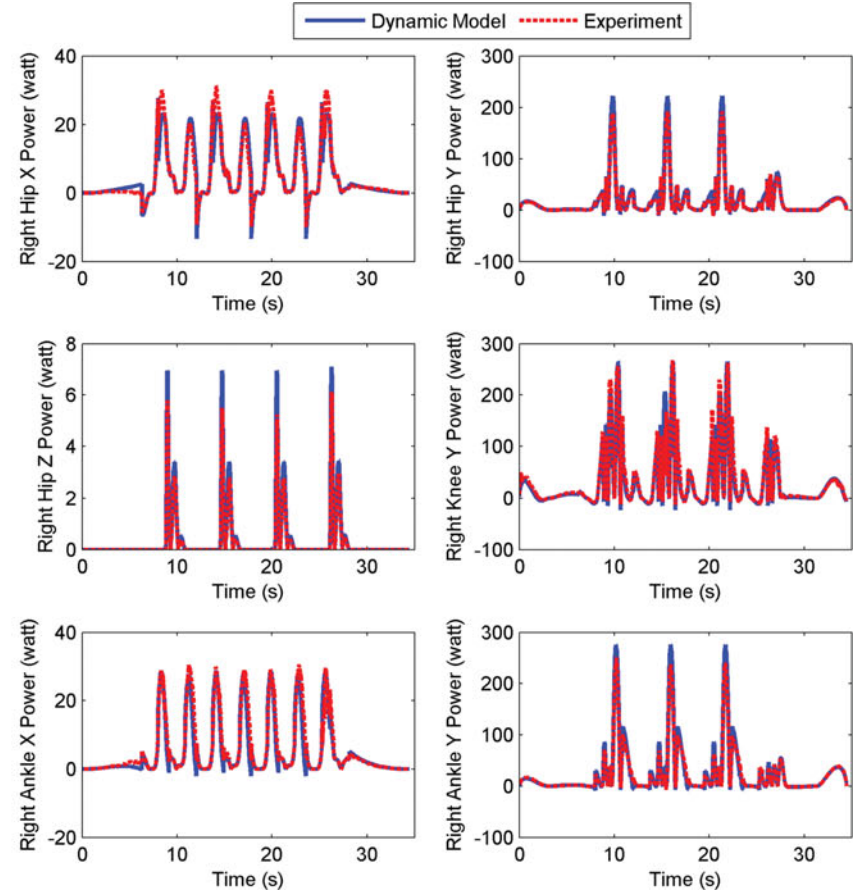


Fig. 13. Right leg joint torques and powers of dynamics model and experiment test.



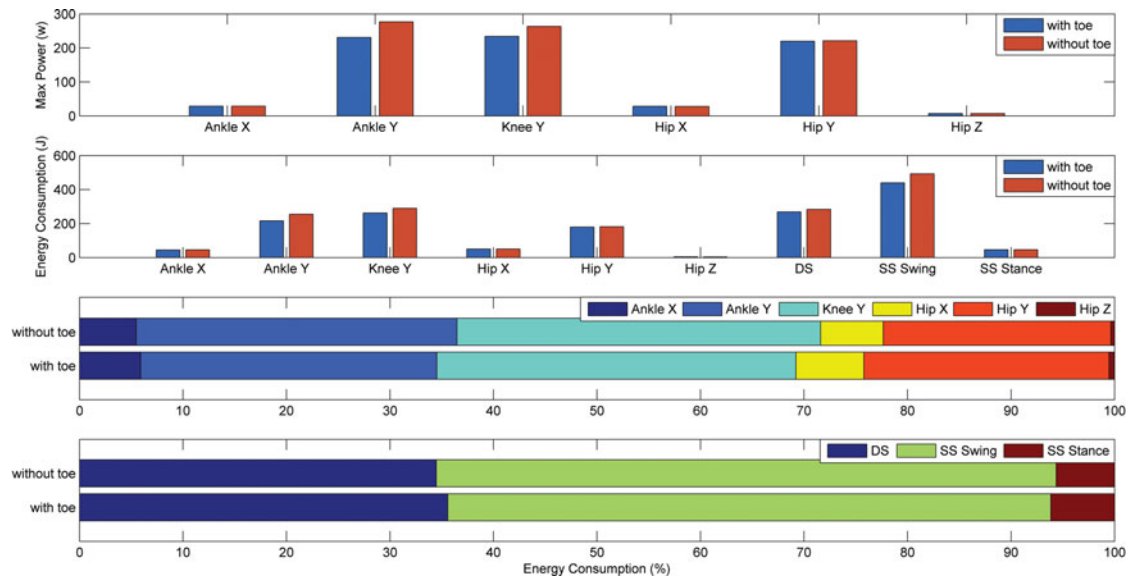


Fig. 14. Comparison of gaits with and without passive toe joints from energy consumption standpoint.

(Fig. 13). It can be seen that the simulation and experimental results are closely matched with a total energy consumption error of 3.5%. This error can be due to the following items:

- (1) Parameter errors such as link mass, moment of inertia and length.
- (2) Parameter identification error of stiffness and damping coefficients.
- (3) Power transmission identification errors including unmodeled dynamics.
- (4) Position following errors of joint actuators in experimental test.

The knee and ankle joints have the maximum torque and power of 219 N.m and 275 J/s, respectively. Also, the hip joint in  $z$ -direction has the minimum torque and power. This joint rotates when the sole is not parallel to the ground, according to IK.<sup>45</sup>

#### 6.4. Benefits of passive toe joint

A comparison between gait of a robot without toe joint and gait of a robot equipped with passive toe joint is presented to emphasize the benefits of implementing passive toe joints. In these gaits, the angle of heel-off and heel strike motions are both  $10^\circ$ . According to Fig. 14, the maximum required power of ankle and knee joints in  $y$  direction reduce 16.6% and 11.4%, respectively. Moreover, energy consumptions of these joints decrease 15.3% and 9.0%, while other joints do not affect much. Zhu *et al.* mentioned 17.6% reduction in energy consumption of ankle joint using passive toe joints.<sup>15</sup>

The most energy consumption reduction is due to the swing phase of SS which is 10.8%. Also, 4.9% less energy consume in DS as well. Implementing passive toe joint balances the energy consumption in different joints and phases of the gait as depicted in Fig. 14. For instance, energy consumption of the ankle joint and energy consumption in the swing phase of SS with respect to the total energy consumption are reduced. This study also confirms Sun *et al.* study, which states that a proper toe actuation mode reduces energy consumption of ankle joints.<sup>16</sup>

#### 6.5. Parametric analysis

In this section, the effects of large values of  $K$  and  $C$  on joint torques and powers are investigated. Several analyses show that stiffness and damping coefficients mainly affect the heel-off motions. Therefore, joint torques and powers for large values of stiffness and damping coefficients in right leg heel-off phase are illustrated in Figs. 15, 16, 17 and 18.

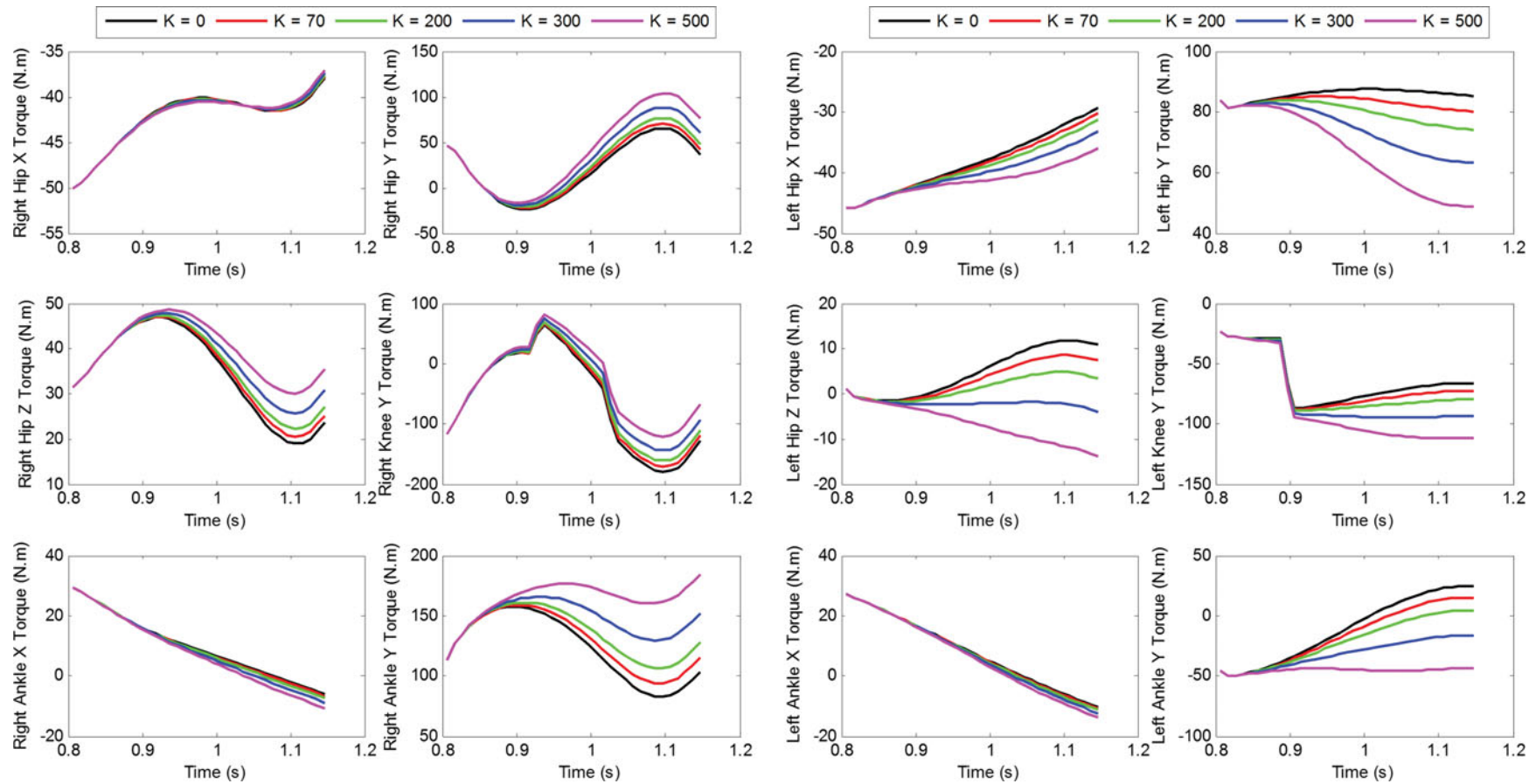


Fig. 15. Effects of large values of  $K$  for  $C = 0.0004$  on joint torques in right leg heel-off motion.



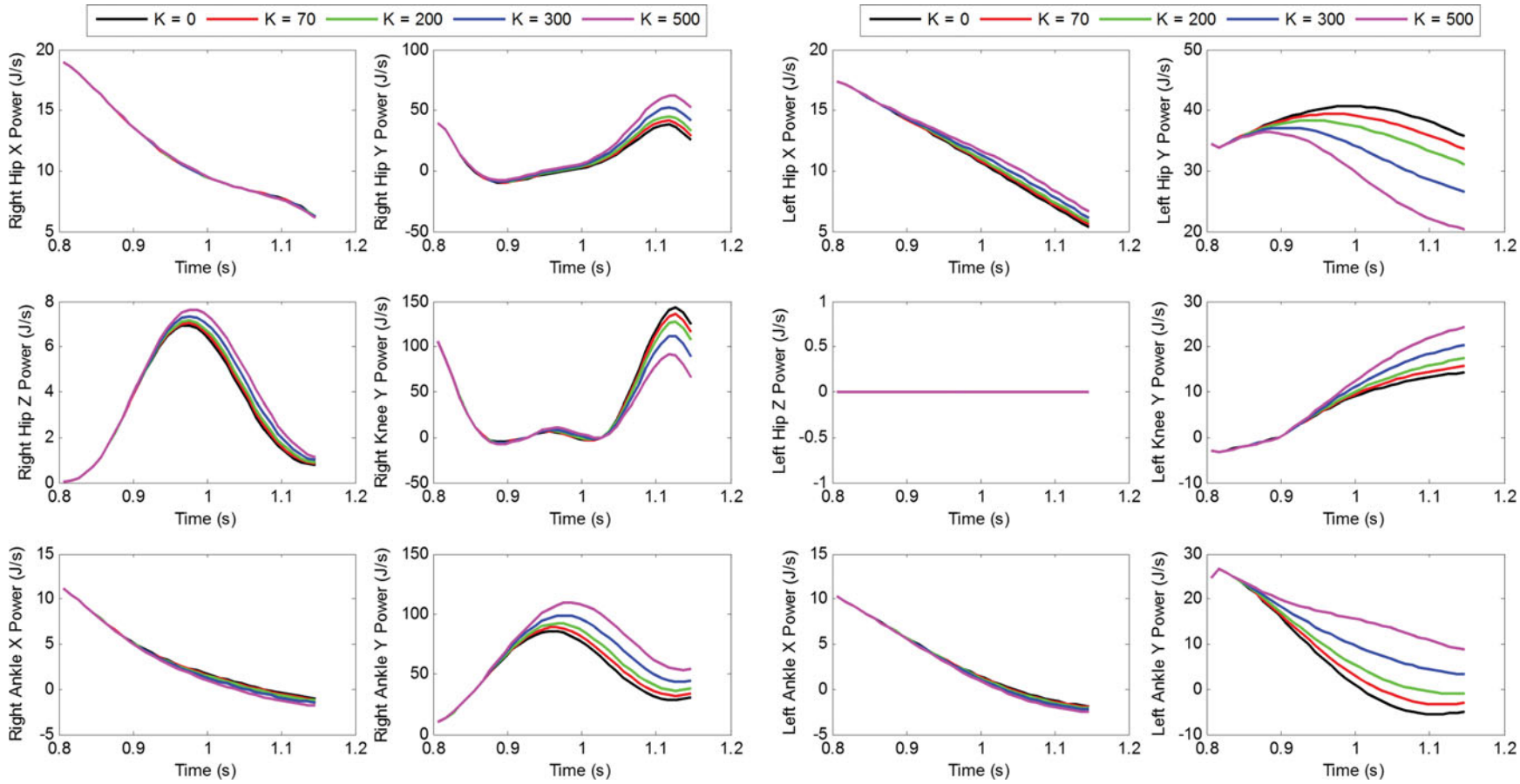


Fig. 16. Effects of large values of  $K$  for  $C = 0.0004$  on joint powers in right leg heel-off motion.

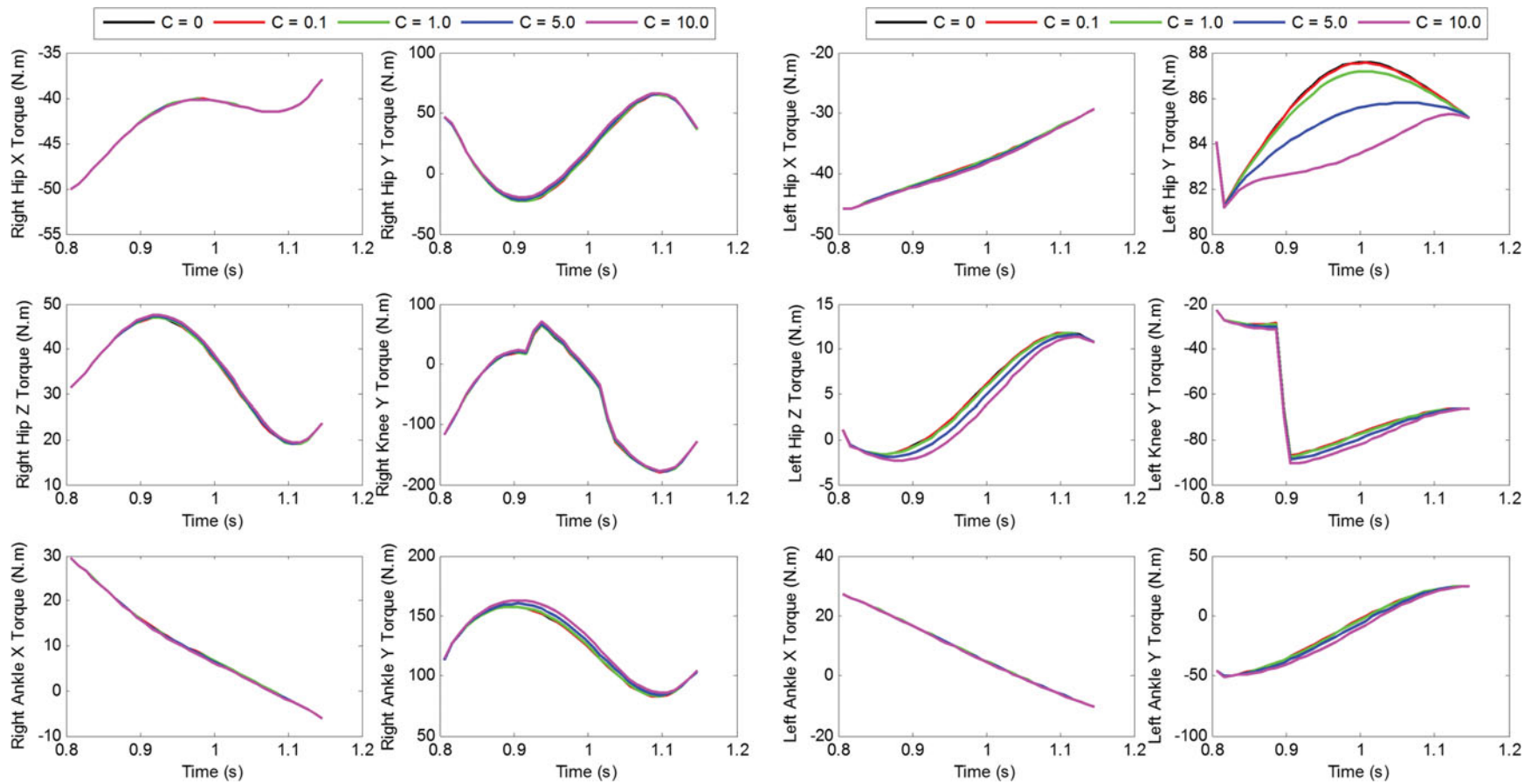


Fig. 17. Effects of large values of  $C$  for  $K = 0.6938$  on joint torques in right leg heel-off motion.

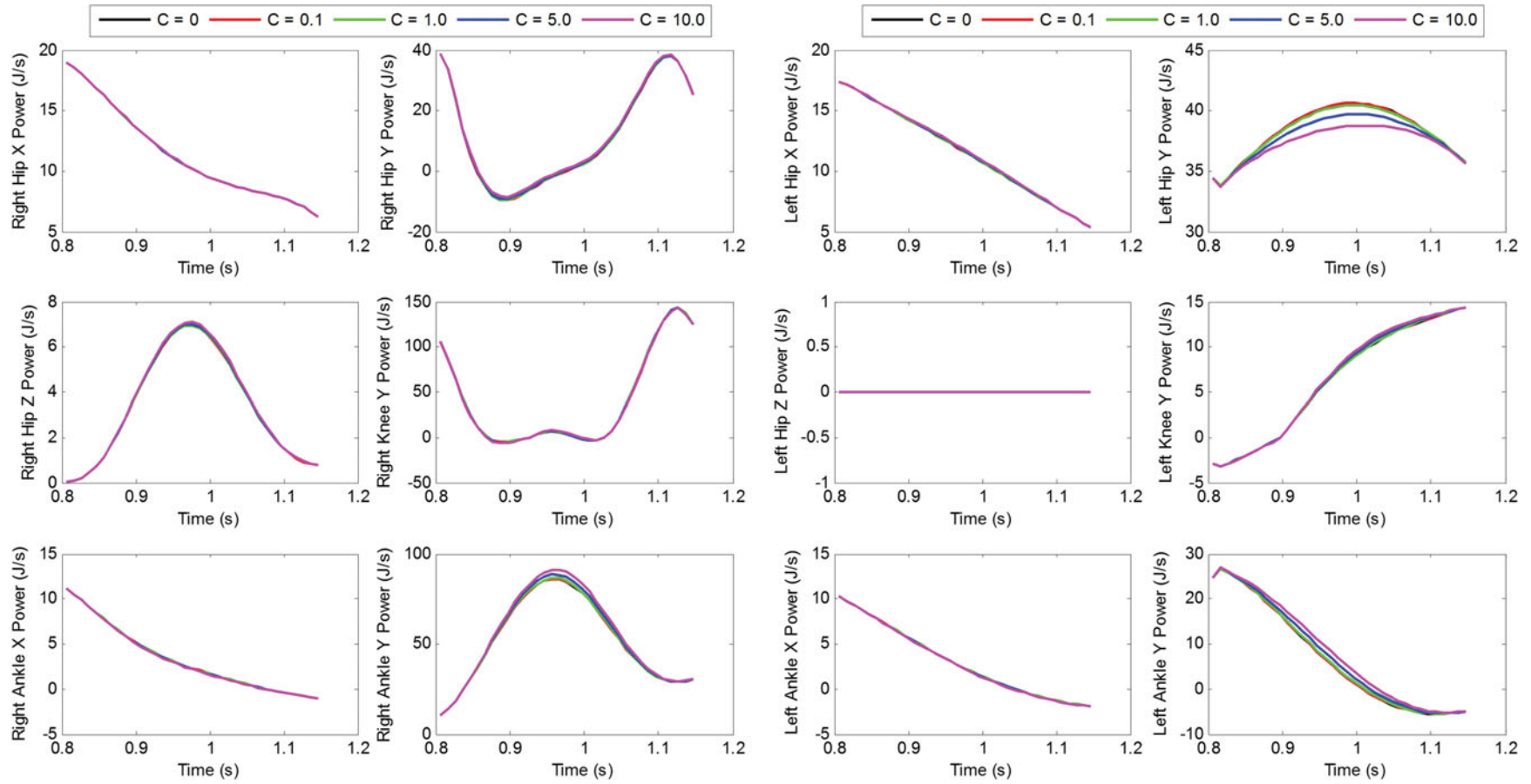


Fig. 18. Effects of large values of  $C$  for  $K = 0.6938$  on joint powers in right leg heel-off motion.

Table IV. Results of using large values of  $K$  and  $C$  on joint torque and powers.

	Right* hip x		Right hip y		Right hip z		Right knee y		Right ankle x		Right ankle y		Left** hip x		Left hip y		Left t hip z		Left knee y		Left ankle x		Left ankle y	
	$K$	$C$	$K$	$C$	$K$	$C$	$K$	$C$	$K$	$C$	$K$	$C$	$K$	$C$	$K$	$C$	$K$	$C$	$K$	$C$	$K$	$C$	$K$	$C$
	Torque	-	-	↑	-	↑	-	↓	-	-	-	↑	↑	↑	-	↓	↓	↓	↓	↑	-	-	-	↑
Power	-	-	↑	-	-	-	↓	-	-	-	↑	↑	-	-	↓	↓	-	-	↑	-	-	-	↑	↑

\*The leg with heel-off motion.

\*\*The stance leg.

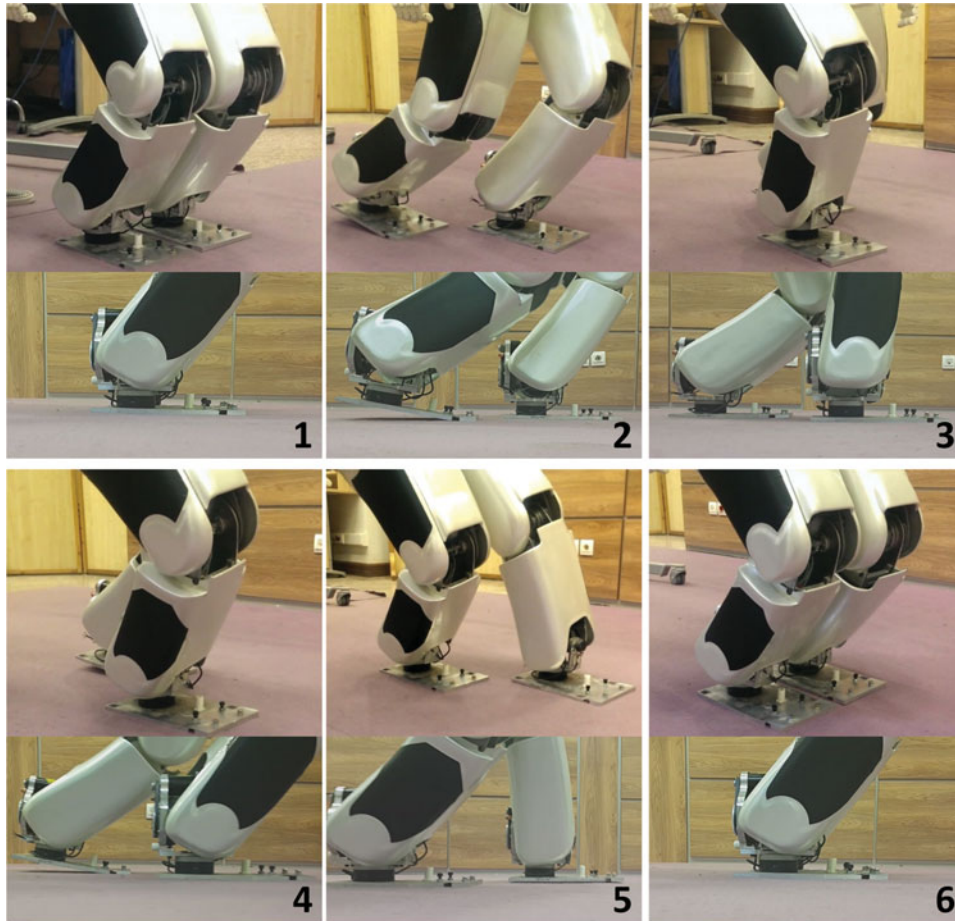


Fig. 19. Snapshots of experimental test of one cycle of gait with 40 cm stride length.

Negative power occurs when the velocity and torque of a joint are in opposite directions. In this case, the regenerated energy is used in other joints by connecting DC bus of the drivers. Although, this process is not ideal, it helps minimize the total energy consumption. The results of using large values of  $K$  and  $C$  on joint torques and powers are summarized in Table IV.

Table IV shows that using passive toe joints with large values of  $K$ , reduces the torque and power of the right knee and the left hip as it increases the torque and power of both ankle joints. On the other hand, large values of  $C$  reduces torque and power of the left hip as it slightly increases torque and power of the right ankle.

In Fig. 19, snapshots of experimental test of one cycle of gait with 40 cm stride length are illustrated.

## 7. Conclusion

In this paper, adding the passive toe joints to SURENA III humanoid robot has been investigated. In order to evaluate the passive toe joint, a simple yet effective mechanism has been designed and fabricated, at first. Then, a free vibration test with vision-based measurement has been adopted to determine the stiffness and damping coefficients of the toe joint. Afterwards, a walking pattern generation routine is presented for humanoid robots equipped with passive toe joints. The stability of the gait has been checked using the ZMP criterion. In this part, the angle of toe joint in the swing phase has been calculated using a base-excited vibration model. Dynamic modeling of the robot with passive toe joints has been developed. The presented model consists of two parts; multi-body dynamics based on the Lagrange approach and power transmission dynamics based on the system identification routine. The stability analysis and the proposed dynamic model have been verified using several simulations and experimental tests on SURENA III humanoid robot. In previous studies, the reduction in ankle energy consumption has been stated as the main benefit of implementing passive toe joints. However, this paper not only confirms the previous investigations, but also indicates that the maximum required power and energy consumption of the knee joint are reduced as well. At the end, parametric analyses have been carried out to study the effects of different values of stiffness and damping coefficients. The obtained results show that using passive toe joints with large  $K$  reduces the required torque and power of the knee and hip joints while increases the ankle joint torque and power. This study provides a better understanding of passive toe joint functionality to generate more natural gaits for humanoid robots.

Hybrid toe joint which is an active toe with a spring and a damper mechanism, can be studied in the future as well. Dynamic modeling and parametric analysis of humanoid robots with this toe joint may be investigated. By comparing energy consumption and required joint torques and powers, the best stiffness and damping coefficients of hybrid toe joint can be calculated.

## Acknowledgements

The authors would like to express deep gratitude to the Industrial Development and Renovation Organization of Iran (IDRO) and Iran National Science Foundation (INSF) for financial supports (Project Number: 94000927) to develop the SURENA III humanoid robot. We further thank the members of the Center of Advanced Systems and Technologies (CAST) for their valuable participation in design and fabrication of SURENA III humanoid robot.

## References

1. K. Nishiwaki, S. Kagami, Y. Kuniyoshi, M. Inaba and H. Inoue, "Toe Joints That Enhance Bipedal and Fullbody Motion of Humanoid Robots," *Proceedings of the ICRA'02, IEEE International Conference on Robotics and Automation*, (IEEE), Washington, DC, USA (2002) pp. 3105–3110.
2. T. Buschmann, S. Lohmeier and H. Ulbrich, "Humanoid robot lola: Design and walking control," *Physiol. Paris* **103**, 141–148 (2009).
3. R. Tajima, D. Honda and K. Suga, "Fast Running Experiments Involving a Humanoid Robot," *Proceedings of the ICRA'09, IEEE International Conference on Robotics and Automation*, (IEEE), Kobe, Japan (2009) pp. 1571–1576.
4. K. Miura, M. Morisawa, F. Kanehiro, S. Kajita, K. Kaneko and K. Yokoi, "Human-Like Walking with Toe Supporting for Humanoids," *IEEE/RSJ International Conference on Intelligent Robots and Systems (IROS)*, (IEEE), San Francisco, CA, USA (2011) pp. 4428–4435.
5. Y. Ogura, K. Shimomura, A. Kondo, A. Morishima, T. Okubo, S. Momoki, H. Lim and A. Takanishi, "Human-Like Walking with Knee Stretched, Heel-Contact and Toe-Off Motion by a Humanoid Robot," *IEEE/RSJ International Conference on Intelligent Robots and Systems*, (IEEE), Beijing, China (2006) pp. 3976–3981.
6. G. Nelson, A. Saunders, N. Neville, B. Swilling, J. Bondaryk, D. Billings, C. Lee, R. Playter and M. Raibert, "Petman: A humanoid robot for testing chemical protective clothing," *Robot. Soc. Japan* **30**, 372–377 (2012).
7. S. Kajita, K. Kaneko, M. Morisawa, S. Nakaoka and H. Hirukawa, "Zmp-Based Biped Running Enhanced by Toe Springs," *IEEE International Conference on Robotics and Automation*, (IEEE), Roma, Italy (2007) pp. 3963–3969.
8. P. Douliez, O. Bruneau and F. Oueddou, "Force control of the redundant leg of a biped robot to produce large inertial effects for crossing obstacles," *Int. J. Humanoid Robot.* **9**, 125–130 (2012).
9. A. Ki, L. Cheol and G. Jo, "Development of a Biped Robot with Toes to Improve Gait Pattern," *IEEE/ASME International Conference on Advanced Intelligent Mechatronics*, (IEEE), Kobe, Japan (2003) pp. 729–734.

10. L. Wang, Z. Yu, Q. Meng and Z. Zhang, "Influence Analysis of Toe-Joint on Biped Gaits," *IEEE International Conference on Mechatronics and Automation*, (IEEE), Luoyang, Henan, China (2006) pp. 1631–1635.
11. E. Kouchaki and M. J. Sadigh, "Effect of Toe-Joint Bending on Biped Gait Performance," *IEEE International Conference on Robotics and Biomimetics (ROBIO)*, (IEEE), Tianjin, China (2010) pp. 697–702.
12. N. Handharu, J. Yoon and G. Kim, "Gait Pattern Generation with Knee Stretch Motion for Biped Robot Using Toe and Heel Joints," *8th IEEE-RAS International Conference on Humanoids*, (IEEE), Daejeon, South Korea (2008) pp. 265–270.
13. M. J. Sadigh, E. Kouchaki and C. Wu, "Effects of constraints on standing balance of a biped with toe-joints," *Int. J. Humanoid Robot.* **9**, 125–136 (2012).
14. R. Sellaouti, O. Stasse, S. Kajita, K. Yokoi and A. Kheddar, "Faster and Smoother Walking of Humanoid Hrp-2 with Passive Toe Joints," *IEEE/RSJ International Conference on Intelligent Robots and Systems*, (IEEE), Daejeon, South Korea (2006) pp. 4909–4914.
15. J. Zhu, Q. Wang and L. Wang, "Effects of Toe stiffness on ankle kinetics in a robotic transtibial prosthesis during level-ground walking," *Mechatronics* **24**, 1254–1261 (2014).
16. S. Sun, Y. Huang and Q. Wang, "Adding adaptable toe stiffness affects energetic efficiency and dynamic behaviors of bipedal walking," *J. Theoretical Biol.* **388**, 108–118 (2016).
17. R. Kumar, N. Handharu, Y. Jungwon and K. Gap-soon, "Hybrid Toe and Heel Joints for Biped/Humanoid Robots for Natural Gait," *Proceeding of the ICCAS'07, International Conference on Control, Automation and Systems*, (ICCAS), Seoul, South Korea (2007) pp. 2687–2692.
18. K. Yamamoto, T. Sugihara and Y. Nakamura, "Toe Joint Mechanism Using Parallel Four-Bar Linkage Enabling Humanlike Multiple Support at Toe Pad and Toe Tip," *7th IEEE-RAS International Conference on Humanoid Robots*, (IEEE), Pittsburg, PA, USA (2007) pp. 410–415.
19. B. Borovac and S. Slavnic, "Design of Multi-Segment Humanoid Robot Foot," *Research and Education in Robotics* (Springer, Berlin, Heidelberg, 2009), pp. 12–18.
20. K. Narioka, T. Homma and K. Hosoda, "Humanlike Ankle-Foot Complex for a Biped Robot," *IEEE-RAS/RSJ International Conference on Humanoid Robots*, (IEEE), Osaka, Japan (2012) pp. 117–125.
21. M. Vukobratović and B. Borovac, "Zero-moment point-thirty five years of its life," *Int. J. Humanoid Robot.* **1**, 157–173 (2004).
22. A. Goswami, "Postural stability of biped robots and the foot-rotation indicator (Fri) point," *Int. J. Robot. Res.* **18**, 523–533 (1999).
23. M. B. Popovic, A. Goswami and H. Herr, "Ground reference points in legged locomotion: Definitions, biological trajectories and control implications," *Int. J. Robot. Res.* **24**, 1013–1032 (2005).
24. H. Hirukawa, S. Hattori, S. Kajita, K. Harada, K. Kaneko, F. Kanehiro, M. Morisawa and S. Nakaoka, "A Pattern Generator of Humanoid Robots Walking on a Rough Terrain," *IEEE International Conference on Robotics and Automation*, (IEEE), Roma, Italy (2007) pp. 2181–2187.
25. W. He, Y. Dong and C. Sun, "Adaptive Neural Impedance Control of a Robotic Manipulator with Input Saturation," *IEEE Trans. Syst. Man Cybern.: Syst.* **46**, 334–344 (2016).
26. W. He, A.O. David, Z. Yin and C. Sun, "Neural Network Control of a Robotic Manipulator with Input Deadzone and Output Constraint," *IEEE Trans. Syst. Man Cybern.: Syst.* **99**, 1–12 (2015).
27. W. He, Y. Chen and Z. Yin, "Adaptive neural network control of an uncertain robot with full-state constraints," *IEEE Trans. Cybern.* **46**, 620–629 (2016).
28. Z. Zhang, Z. Li, Y. Zhang, Y. Luo and Y. Li, "Neural-dynamic-method-based dual-arm cmg scheme with time-varying constraints applied to humanoid robots," *IEEE Trans. Neural Netw. Learning Syst.* **26**, 3251–3262 (2015).
29. G. Carbone, Y. Ogura, H. Lim, A. Takanishi and M. Ceccarelli, "Dynamic simulation and experiments for the design of a new 7-dofs biped walking leg module," *Robotica* **22**, 41–50 (2004).
30. P. Channon, S. Hopkins and D. Pham, "Derivation of optimal walking motions for a bipedal walking robot," *Robotica* **10**, 165–172 (1992).
31. C. Chevallereau and Y. Aoustin, "Optimal reference trajectories for walking and running of a biped robot," *Robotica* **19**, 557–569 (2001).
32. M. Rostami and G. Bessonnet, "Sagittal gait of a biped robot during the single support phase. part 2: Optimal motion," *Robotica* **19**, 241–253 (2001).
33. T. Saidouni and G. Bessonnet, "Generating globally optimised sagittal gait cycles of a biped robot," *Robotica* **21**, 199–210 (2003).
34. M. J. Sadigh and S. Mansouri, "Application of phase-plane method in generating minimum time solution for stable walking of biped robot with specified pattern of motion," *Robotica* **31**, 837–851 (2013).
35. X. Zhou, Y. Guan, L. Jiang, H. Zhu, C. Cai, W. Wu and H. Zhang, "Stability of biped robotic walking with frictional constraints," *Robotica* **31**, 573–588 (2013).
36. M. Khadiv, S.A.A. Moosavian, A. Yousefi-Koma, M. Sadedel and S. Mansouri, "Optimal gait planning for humanoids with 3d structure walking on slippery surfaces," *Robotica*, 1–19 (2015).
37. S. Aoi and K. Tsuchiya, "Generation of bipedal walking through interactions among the robot dynamics, the oscillator dynamics, and the environment: Stability characteristics of a five-link planar biped robot," *Auton. Robots* **30**, 123–141 (2011).

38. M. Sadedel, A. Yousefi-Koma and M. Khadiv, "Offline Path Planning, Dynamic Modeling and Gait Optimization of a 2d Humanoid Robot," *2nd RSI/ISM International Conference on Robotics and Mechatronics (ICRoM)*, (IEEE), Tehran, Iran (2014) pp. 131–136.
39. M. Khadiv, S. A. Moosavian and M. Sadedel, "Dynamics Modeling of Fully-Actuated Humanoids with General Robot-Environment Interaction," *2nd RSI/ISM International Conference on Robotics and Mechatronics (ICRoM)*, (IEEE), Tehran, Iran (2014) pp. 233–238.
40. B. Ugurlu, J. Saglia, N. Tsagarakis and D. Caldwell, "Yaw moment compensation for bipedal robots via intrinsic angular momentum constraint," *Int. J. Humanoid Robot.* **9**, 1250033 (2012).
41. T. Wang, C. Chevallereau and C. Rengifo, "Walking and steering control for a 3d biped robot considering ground contact and stability," *Robot. Auton. Syst.* **60**, 962–977 (2012).
42. Y. Aoustin and A. Formalskii, "3d walking biped: Optimal swing of the arms," *Multibody Syst. Dyn.* **32**, 55–66 (2014).
43. M. Sadedel, A. Yousefikoma and F. Iranmanesh, "Analytical dynamic modelling of heel-off and toe-off motions for a 2d humanoid robot," *J. Comput. Appl. Mech.* **46**, 243–256 (2015).
44. D. Inman, *Engineering Vibration (3rd)*. (Pearson, ISBN 0-13-228173-2, Upper Saddle River, NJ, 2007).
45. J. Nunez, A. Briseno, D. Rodriguez, J. Ibarra and V. Rodriguez, "Explicit Analytic Solution for Inverse Kinematics of Bioloid Humanoid Robot," *Robotics Symposium and Latin American Robotics Symposium (SBR-LARS)*, (IEEE), Washington, DC, USA (2012) pp. 33–38.
46. Q. Huang and Y. Nakamura, "Sensory reflex control for humanoid walking," *IEEE Trans. Robot.* **21**, 977–984 (2005).
47. H. Baruh, *Analytical Dynamics*, (WCB/McGraw-Hill, Boston, 1999).
48. A. Ben and T. Greville, *Generalized Inverses: Theory and Applications*, vol. 15 (Springer Science & Business Media, New York, USA, 2003).
49. J. Grcar, "How ordinary elimination became gaussian elimination," *Historia Math.* **38**, 163–218 (2011).
50. H. Taghirad and P. Belanger, "Modeling and parameter identification of harmonic drive systems," *J. Dyn. Syst. Meas. Control Trans.-Am. Soc. Mech. Eng.* **120**, 439–444 (1998).